ICES REPORT 16-05

February 2016

Discontinuous and enriched Galerkin methods for phase-field fracture propagation in elasticity

by

Prashant Mital, Thomas Wick, Mary F. Wheeler, Gergina Pencheva

Discontinuous and enriched Galerkin methods for phase-field fracture propagation in elasticity

Prashant Mital [*]   Thomas Wick [†]   Mary F. Wheeler [‡]   Gergina Pencheva [§]

In this work, we introduce discontinuous Galerkin and enriched Galerkin formulations for the spatial discretization of phase-field fracture propagation. The nonlinear coupled system is formulated in terms of the Euler-Lagrange equations, which are subject to a crack irreversibility condition. The resulting variational inequality is solved in a quasi-monolithic way in which the irreversibility condition is incorporated with the help of an augmented Lagrangian technique. The relaxed nonlinear system is treated with Newton's method. Numerical results complete the present study.

Keywords: Phase field fracture; Discontinuous Galerkin; SIPG; NIPG; IIPG; augmented Lagrangian method

1 Introduction

Fracture propagation in elasticity, plasticity, and porous media is currently one of the major research topics in mechanical, energy, and environmental engineering. In this paper, we concentrate specifically on fracture propagation in elasticity. We consider a variational approach for brittle fracture introduced in [6], which has been later formulated in terms of a thermodynamically-consistent phase field technique [8]. In fact, variational and phase field formulations for fracture are active research areas as attested in recent years, e.g., [3, 9, 2, 4, 1, 10]. Our motivations for employing a phase field model are that fracture nucleation, propagation, kinking, and curvilinear paths are automatically included in the model; post-processing of stress intensity factors and remeshing resolving the crack path are avoided. Furthermore, the underlying equations are based on continuum mechanics principles that can be treated with adaptive Galerkin finite elements.

In this work, we extend existing Galerkin formulations for phase-field fracture with regard to two major aspects:

- Spatial discretization of the displacement field with discontinuous Galerkin (DG) finite elements resulting in NIPG [12] and IIPG methods [5] and an enriched Galerkin (EG) formulation [13];

- Formulation of a quasi-monolithic augmented Lagrangian iteration for the nonlinear coupled displacement-phase-field system.

These frameworks are formulated in Sections 2 - 4 and are substantiated with numerical tests in Section 5.

[*]Center for Subsurface Modeling, The Institute for Computational Engineering and Sciences, The University of Texas at Austin, Austin, Texas 78712, USA

[†]RICAM, Austrian Academy of Sciences Altenberger Str. 69 4040 Linz, Austria

[‡]Center for Subsurface Modeling, The Institute for Computational Engineering and Sciences, The University of Texas at Austin, Austin, Texas 78712, USA

[§]Center for Subsurface Modeling, The Institute for Computational Engineering and Sciences, The University of Texas at Austin, Austin, Texas 78712, USA

2 The phase-field fracture model

We limit our attention to 2-dimensional problems and let $\Omega \in \mathbb{R}^2$, be a smooth, open, connected and bounded set. We denote the L^2 scalar product with $(\cdot, \cdot)$, and assume that the crack $\mathcal{C}$ is a 1-dimensional set, not necessarily connected, contained in Ω. Using the variational/phase-field approach to fracture [6, 3], the crack $\mathcal{C}$ is represented using a continuous phase field variable $\varphi : \Omega \to [0, 1]$. This value of the phase field variable interpolates between the broken ($\varphi = 0$) and unbroken ($\varphi = 1$) states of the material. The diffusive transition zone between these two states is controlled by a regularization parameter $\varepsilon > 0$. Imposing a crack irreversibility condition $\varphi \leq \varphi^{n-1}$ (where $\varphi^{n-1} := \varphi(t^{n-1})$) denotes the previous time step solution), and further ingredients for a thermodynamically consistent phase-field framework [8] result in the following Euler-Lagrange formulation:

Formulation 1: Find vector-valued displacements and a scalar-valued phase-field variable $(\mathbf{u}, \varphi) \in \{\bar{\mathbf{u}} + V\} \times W$ such that

$$\Big(\big((1 - \kappa)\varphi^2 + \kappa\big)\sigma(\mathbf{u}), e(\mathbf{w}) \Big) = 0 \quad \forall \mathbf{w} \in V, \tag{1}$$

as well as,

$$(1 - \kappa)(\varphi\sigma(\mathbf{u}) : e(\mathbf{u}), \psi - \varphi)$$
$$+ G_c\left(-\frac{1}{\varepsilon}(1 - \varphi, \psi - \varphi) + \varepsilon(\nabla\varphi, \nabla\psi - \varphi) \right) \geq 0 \quad \forall \psi \in W_{in} \cap L^\infty(\Omega), \tag{2}$$

where $V := H_0^1(\Omega)$, $W_{in} := \{w \in H^1(\Omega) | w \leq \varphi^{n-1} \leq 1 \text{ a.e. on } \Omega\}$ and $W := H^1(\Omega)$. Furthermore, $\sigma = \sigma(\mathbf{u}) = 2\mu_s e + \lambda_s tr(e)I$ is the stress tensor with $\mu_s, \lambda_s > 0$, and $e(\mathbf{u}) = 0.5(\nabla\mathbf{u} + \nabla\mathbf{u}^T)$ is the linearized strain tensor. The critical energy release rate is $G_c > 0$. The domain is subject to boundary conditions, and we assume $\Gamma_D \neq \emptyset$, with the possibly non-homogeneous and time-dependent Dirichlet boundary conditions $\bar{\mathbf{u}}$. Moreover, κ is a regularization parameter for the elastic energy bounded below by 0, such that $\kappa \ll \varepsilon$, see e.g., [3].

To treat crack irreversibility, we use the augmented-Lagrangian formulation described in [14]. To apply this method, we begin by approximating the time derivative $\partial_t \varphi$ using the backward difference

$$\partial_t \varphi \approx \partial_{\Delta t} \varphi = \frac{\varphi - \varphi^{n-1}}{\Delta t} \quad \Rightarrow \quad \frac{1}{\Delta t}\Big((\lambda + \gamma(\varphi - \varphi^{n-1}))^+ \Big), \quad \Delta t = t^n - t^{n-1}.$$

Here, λ and γ are a penalization function and parameter, respectively, and φ^{n-1} is the phase field solution at the previous time step. Moreover, $(x)^+ := \max\{0, x\}$.

3 A quasi-monolithic incremental formulation

We choose a quasi-monolithic approach [7] as this reduces algorithmic complexity and has been demonstrated to be numerically robust and efficient when φ is replaced by the extrapolation $\tilde{\varphi}$ in the first term of Formulation 2. The reason for choosing $\tilde{\varphi}$ is the need to circumvent the non-convexity of the underlying energy functional.

Algorithm 1 Solution algorithm

For each time t^n:
Let $m = 0$; choose initial $\lambda_m \in L^2(\Omega)$, $\gamma > 0$.
repeat
    Let $k = 0$; choose initial $\tilde{U}_k \in V_h \times W_h$.
    repeat
        Find δU_k solving $A'(U_k)(\delta U_k, \Psi) = -A(U_k)(\Psi)$
        Update $\tilde{U}_{k+1} \leftarrow \tilde{U}_k + \delta U_k$
        Update $k \leftarrow k + 1$
    until Stopping criterion $\|U_k - U_{k-1}\| \leq \text{TOL}_2$ is satisfied.
    Set $U_{m+1} = (\mathbf{u}_{m+1}, \varphi_{m+1}) = \tilde{U}_k$
    Update $\lambda_{m+1} = \min(0, \lambda_m + \gamma\varphi_{m+1}) + (\lambda_m + \gamma(\varphi_{m+1} - \varphi^{n-1}))^+$
    Update $m \leftarrow m + 1$
until Stopping criterion $\max(\|\mathbf{u}_{m-1} - \mathbf{u}_m\|, \|\lambda_{m-1} - \lambda_m\|) \leq \text{TOL}_i$ is satisfied.
$(\mathbf{u}^n, \varphi^n) = (\mathbf{u}_{m+1}, \varphi_{m+1})$

Formulation 2: Find $U := \{\mathbf{u}, \varphi\} \in \{\bar{\mathbf{u}} + V\} \times W$, where $V := H_0^1(\Omega)$ and $W := H^1(\Omega)$, such that

$$A(U)(\Psi) = 0 \quad \forall \Psi := \{\mathbf{w}, \psi\} \in V \times W, \tag{3}$$

where $A(\cdot)(\cdot)$ is the following semi-linear form

$$A(U)(\Psi) = \left(\left((1 - \kappa)\tilde{\varphi}^2 + \kappa\right)\sigma(\mathbf{u}), e(\mathbf{w})\right) + (1 - \kappa)(\varphi\sigma(\mathbf{u}) : e(\mathbf{u}), \psi)$$
$$+ G_c\left(-\frac{1}{\varepsilon}(1 - \varphi, \psi) + \varepsilon(\nabla\varphi, \nabla\psi)\right) + \frac{1}{\Delta t}\left((\lambda + \gamma(\varphi - \varphi^{n-1}))^+, \psi\right). \tag{4}$$

Here $\tilde{\varphi}$ is a linear extrapolation of time-lagged φ, i.e. $\varphi \approx \tilde{\varphi} := \tilde{\varphi}(\varphi^{n-1}, \varphi^{n-2})$, with $\varphi^{n-1}, \varphi^{n-2}$ denoting solutions to previous time steps. Solving the nonlinear variational problem (4) is performed with Newton's method and line search backtracking. The resulting solution algorithm is outlined in Algorithm 1.

4 Spatial discretization with DG and EG

In this section we establish key notations for DG and EG followed by the mathematical statement of the discrete variational forms. On a conforming subdivision $\mathcal{E}_h$ of a polygonal domain Ω subdivided into elements E we define the discontinuous finite element subspace to be

$$\mathcal{D}_k(\mathcal{E}_h) = \{v \in L^2(\Omega) : \forall E \in \mathcal{E}_h, v|_E \in \mathbb{P}_k(E)\}, \tag{5}$$

where $\mathbb{P}_k(E)$ denotes the space of piecewise polynomials of total degree less than or equal to k on E. We also define the space of CG approximating polynomials enriched with discontinuous piecewise constants

$$\mathcal{D}_k^{C0}(\mathcal{E}_h) := \mathcal{D}_k^C(\mathcal{E}_h) \cup \mathcal{D}_0(\mathcal{E}_h). \tag{6}$$

Here $\mathcal{D}_k^C(\mathcal{E}_h)$ is the CG approximating space defined as

$$\mathcal{D}_k^C(\mathcal{E}_h) = \{v \in C(\Omega) : \forall E \in \mathcal{E}_h, v|_E \in \mathbb{P}_k^C(E), v|_{\Gamma_D} = 0\}, \tag{7}$$

3

where $\mathbb{P}_k^C(E)$ denotes the space of continuous piecewise polynomials of total degree less than or equal to k on E.
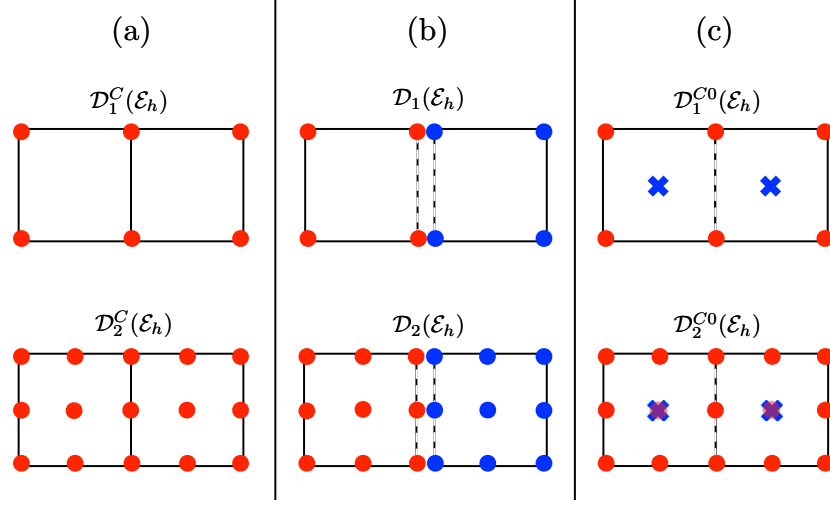

Figure 1: Support points for bilinear and biquadratic basis functions. (a) CG: all support points in red. (b) DG: support points for left element in red, for right element in blue. The common edge has two sets of support points - one from each element. (c) EG: support points from CG approximating space in red, piecewise constants in blue. Only the piecewise constant degree of freedom is discontinuous across the common edge.

In order to describe the vector-valued displacements, we consider the spaces of vector functions that generalize (5) and (6): $\boldsymbol{\mathcal{D}}_k(\mathcal{E}_h) = (\mathcal{D}_k(\mathcal{E}_h))^d$, $\boldsymbol{\mathcal{D}}_k^{C0}(\mathcal{E}_h) = (\mathcal{D}_k^{C0}(\mathcal{E}_h))^d$, where d is the number of spatial dimensions. We note that the functions in $\boldsymbol{\mathcal{D}}_k(\mathcal{E}_h)$ and $\boldsymbol{\mathcal{D}}_k^{C0}(\mathcal{E}_h)$ are discontinuous along the edges (or faces) of the mesh.

Now, consider two neighboring elements E_1^e and E_2^e that share a common side e. Naturally then, there are two traces of $w \in \mathcal{D}_k(\mathcal{E}_h)$ along e. We consider $\mathbf{n}_e$ to be the normal vector associated with e to be oriented from E_1^e to E_2^e and define: $\{\mathbf{w}\} = \frac{1}{2}(\mathbf{w}|_{E_1^e}) + \frac{1}{2}(\mathbf{w}|_{E_2^e})$, $[\mathbf{w}] = (\mathbf{w}|_{E_1^e}) - (\mathbf{w}|_{E_2^e})$ $\forall e = \partial E_1^e \cap \partial E_2^e$. We extend this definition to elements on the boundary $\partial \Omega$ as: $\{\mathbf{w}\} = [\mathbf{w}] = (\mathbf{w}|_{E_1^e})$ $\forall e = \partial E_1^e \cap \partial \Omega$. Further, we denote by $|e|$ the length of an edge e in $d = 2$. We now state the equations corresponding to a discontinuous spatial discretization directly from inspection of the monolithic formulation (4) and the DG-scheme for pure linear elasticity, e.g., [11]. We pursue a discontinuous representation of the displacement variable $\mathbf{u}$ only, recognizing that the regularization in the case of the phase field variable φ enforces its continuity across the crack.

We augment (4) with the jump and penalization terms to define the discrete incremental semi-linear form

$$
\begin{aligned}
A(U_h)(\Psi_h) &= \sum_{E \in \mathcal{E}_h} \int_E \left((1 - \kappa)\tilde{\varphi}^2 + \kappa \right) \sigma(\mathbf{u}), e(\mathbf{w}) \right) \\
&- \sum_{e \in \Gamma_h \cup \Gamma_D} \int_e \{((1 - \kappa)\tilde{\varphi}^2 + \kappa)\sigma(\mathbf{u}) \cdot \mathbf{n}_e\}[\mathbf{w}] + \eta \sum_{e \in \Gamma_h} \int_e \{((1 - \kappa)\tilde{\varphi}^2 + \kappa)\sigma(\mathbf{w}) \cdot \mathbf{n}_e\}[\mathbf{u}] \\
&+ \eta \sum_{e \in \Gamma_D} \int_e \left(((1 - \kappa)\tilde{\varphi}^2 + \kappa)\sigma(\mathbf{w}) \cdot \mathbf{n}_e \right)(\mathbf{u} - \mathbf{g}_D) + \sum_{e \in \Gamma_h} \frac{\delta_e}{|e|^\beta} \int_e [\mathbf{u}][\mathbf{w}] + \sum_{e \in \Gamma_D} \frac{\delta_e}{|e|^\beta} \int_e (\mathbf{u} - \mathbf{g}_D)\mathbf{w} \\
&+ (1 - \kappa)(\varphi\sigma(\mathbf{u}) : e(\mathbf{u}), \psi) + G_c \left(-\frac{1}{\varepsilon}(1 - \varphi, \psi) + \varepsilon(\nabla\varphi, \nabla\psi) \right) + \frac{1}{\Delta t} \left((\lambda + \gamma(\varphi - \varphi^{n-1}))^+, \psi \right),
\end{aligned}
\tag{8}
$$

where $\eta = 1$ (NIPG) or $\eta = 0$ (IIPG); and $\delta_e > 0$ and $\beta > 0$ (here $\beta = 1$) are the DG-penalization and

superpenalization parameters, respectively.

The DG-CG variational problem reads: Find $U_h := \{\mathbf{u}, \varphi\} \in \{\bar{\mathbf{u}}_h + V_h^{DG}\} \times W_h^{CG}$ such that

$$A(U_h)(\Psi_h) = 0 \quad \forall \Psi_h := \{\mathbf{w}, \psi\} \in V_h^{DG} \times W_h^{CG}. \tag{9}$$

The EG-CG variational problem reads: Find $U_h := \{\mathbf{u}, \varphi\} \in \{\bar{\mathbf{u}}_h + V_h^{EG}\} \times W_h^{CG}$ such that

$$A(U_h)(\Psi_h) = 0 \quad \forall \Psi_h := \{\mathbf{w}, \psi\} \in V_h^{EG} \times W_h^{CG}. \tag{10}$$

The test and trial spaces are $V_h^{DG} := [\mathcal{D}_k(\mathcal{E}_h)]^2, V_h^{EG} := [\mathcal{D}_k^{C0}(\mathcal{E}_h)]^2, W_h^{CG} := \mathcal{D}_k^C(\mathcal{E}_h)$. Our formulation enforces both Dirichlet and Neumann boundary conditions weakly. The use of homogeneous Neumann boundary conditions for $\mathbf{u}$ and φ results in a formulation exclusively dependent on Γ_D. The directional derivative of (8) needed for the Newton iterations is computed analytically.

5 A numerical test: single edge notched tension

The single edge notched tension test is a widely used experimental methodology used to characterize the fracture toughness of various materials in plane-strain.
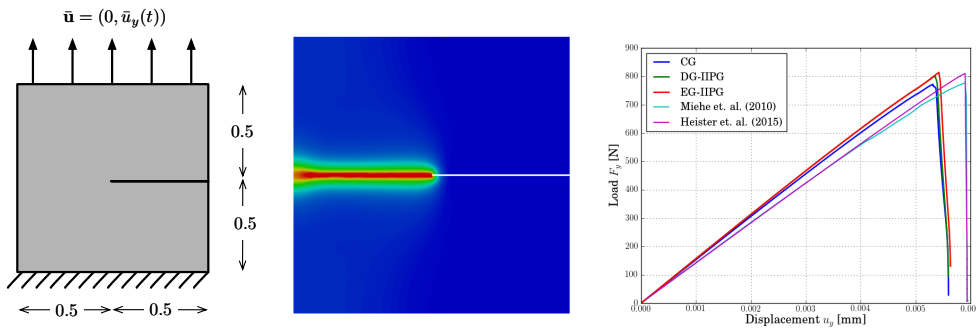

Figure 2: Schematic of the single-edge-notched tension test (left), the final phase-field crack pattern at $T = 6.6 \times 10^{-3}s$ (middle), and comparison of load-displacement curves from our monolithic scheme with CG, DG-IIPG and EG-IIPG against results reported by Miehe et al. [9] and Heister et al. [7].

We consider a square plate with a horizontal notch placed at half-height, running from the right outer surface to the center of the specimen. The plate is subject to zero displacement boundary conditions on the bottom surface, and time-dependent displacement on the top surface. The left and right surfaces are considered to be traction-free. The problem setup is shown in Figure 2. The material parameters are chosen as $\lambda = 121.1538\text{kN/mm}^2$, $\mu = 80.7692\text{kN/mm}^2$ and $G_c = 2.7 \times 10^{-3}\text{kN/mm}$. The displacement boundary condition on the top surface is taken to be $\bar{u}_y(t) = t\bar{\alpha}$ with $\bar{\alpha} = 1$ mm/s. The expected response of this test is the build-up of the stress concentration in the vicinity of the crack-tip, followed by unstable, catastrophic crack growth.

Our first objective is to study h-convergence for fixed ε. We choose $\Delta t = 1.0 \times 10^{-4}s$ for the first 50 loading steps, after which $\Delta t = 1.0 \times 10^{-5}s$. This adaptivity in the time step is necessary to capture the rapid movement of the crack tip. We choose $\varepsilon = 4.4 \times 10^{-2}mm$, $\kappa = 1.0 \times 10^{-12}$, and run our code for $h_1 = 4.4 \times 10^{-2}mm$, $h_2 = 2.2 \times 10^{-2}mm$, and $h_3 = 1.1 \times 10^{-2}mm$. We evaluate the surface load vector on the top surface of Ω as $\tau = (F_x, F_y) = \int_{\partial\Omega_{\text{top}}} \sigma(\mathbf{u})\mathbf{n}ds$. In this example, we are particularly interested in F_y. Our findings for the surface load evolution with varying h are shown in Figure 3 for the IIPG flavors of EG and DG. It is observed

that our approach is stable with spatial mesh refinement, and that our solution converges as we use finer meshes. Comparison to literature values are displayed in Figure 2 at right.
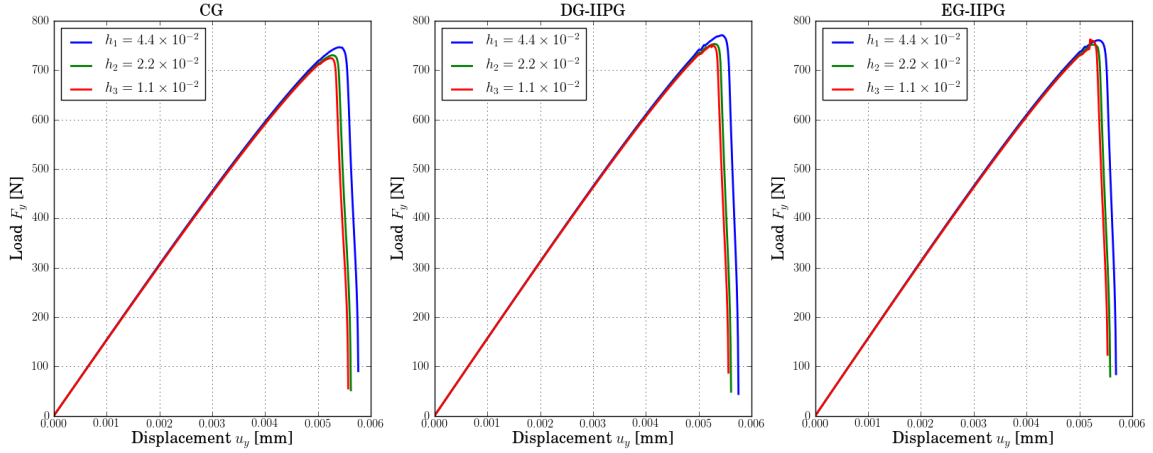

Figure 3: We fix κ and ε on the coarsest mesh level and vary h. Left: CG. Middle: DG-IIPG. Right: EG-IIPG. Spatial convergence is observed for all schemes.

Results obtained from DG-NIPG and EG-NIPG are very similar and are therefore not presented here. The SIPG method ($\eta = -1$) yields unsatisfactory findings, which are not shown in this work.

With the results of our scheme duly validated, we proceed to study the relative efficiency of the schemes by comparing the number of Newton iterations taken by each of them to converge. We first investigate the variation in the number of Newton steps taken with the penalization parameter δ_e. Note that when we multiply Equations (8) throughout by Δt, our effective penalization of the jump becomes $\delta_e \Delta t$. This is an important detail that cannot be overlooked while using DG/EG for the phase field equations because for instance, using $\delta_e = 10^5$ with $\Delta t = 1 \times 10^{-5} s$ gives an effective penalization of $\delta_e \Delta t = 1$ which is not sufficiently large and produces spurious results. In the case of an adaptive time step size (we usually take $\Delta t = 1 \times 10^{-4} s$ for the first 50 steps, and a smaller time step thereafter), the product $\delta_e \Delta t$ is reported for the smaller time step. We vary the values of the effective penalization and plot the cumulative number of Newton steps as a function of time for $h = 1.1 \times 10^{-2} mm$, $\varepsilon = 2h[mm]$, and $\kappa = 1.0 \times 10^{-12}$. The results of this study with IIPG and NIPG are shown in Figure 4. In Figure 5, we observe that DG and EG schemes take much fewer Newton iterations to converge than CG especially after the onset of crack growth (approximately $t = 0.0055s$).
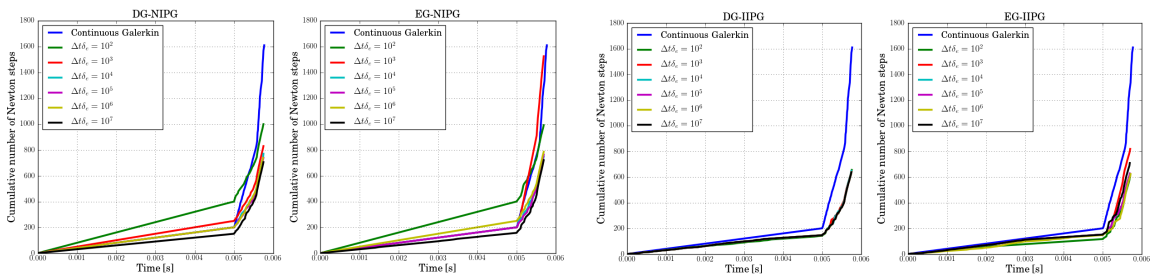

Figure 4: Newton convergence performance with $h = 1.1 \times 10^{-2} mm$, $\Delta t = \{10^{-4}, t < 0.005; 10^{-5}, t \geq 0.005\}$, $\varepsilon = 2h[mm]$, and $\kappa = 10^{-12}$ and varying penalty δ_e. Left: DG-NIPG. Right: EG-NIPG. Left: DG-IIPG. Right: EG-IIPG. Convergence is faster for higher values of penalization.

For a better comparison of the efficiency, we run a test with the same physical parameters as above, but with
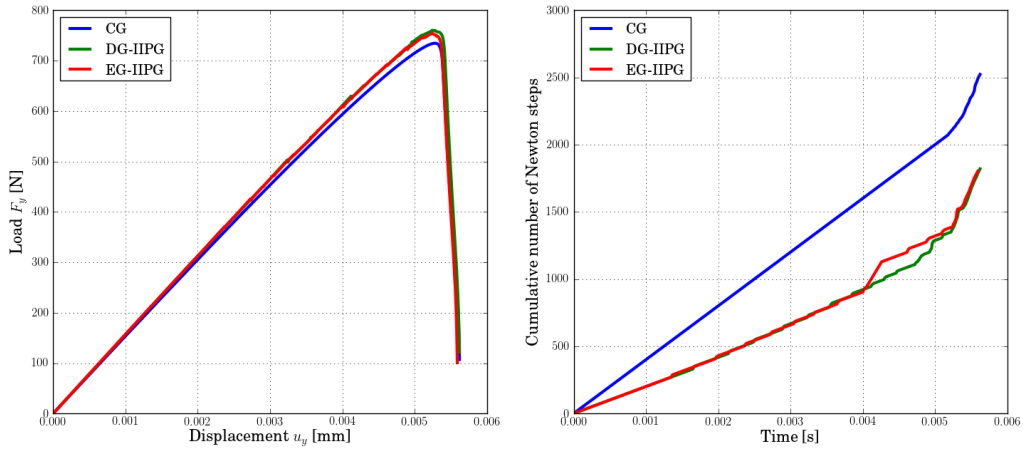
Figure 5: Single edge notched tension test results using CG, DG-IIPG and EG-IIPG. Left: load vs. displacement curve. Right: Newton convergence performance for constant $\Delta t = 10^{-5} s$.

a uniform time step of $\Delta t = 10^{-5} s$ throughout. The motivation is to suppress the effect of adaptive time stepping on the Newton performance and to give an unbiased comparison. Since the computational burden with such a simulation is significant, we only consider the IIPG case with $\delta_e \Delta t = 10^2$. These results are shown in Figure 5. As we can see, DG and EG take roughly the same number of Newton iterations (1800) while CG takes significantly more (2520). We also observe that the load-displacement curves for all three methods are in reasonable agreement. Hence, we can conclusively state that the Newton method converges in fewer iterations for the DG and EG schemes than for the CG scheme. Furthermore by inspecting Figure 1, we see that EG has significantly fewer degrees of freedom than DG.

References

[1] M. Ambati, T. Gerasimov, and L. De Lorenzis, *A review on phase-field models of brittle fracture and a new fast hybrid formulation*, Computational Mechanics **55**:2 (2015), 383–405.

[2] M. J. Borden, C. V. Verhoosel, M. A. Scott, T. J. Hughes, and C. M. Landis, *A phase-field description of dynamic brittle fracture*, Computer Methods in Applied Mechanics and Engineering **217** (2012), 77–95.

[3] B. Bourdin, G. A. Francfort, and J. J. Marigo, *The variational approach to fracture*, Journal of elasticity **91**:1-3 (2008), 5–148.

[4] S. Burke, C. Ortner, and E. Süli, *An adaptive finite element approximation of a variational model of brittle fracture*, SIAM Journal on Numerical Analysis **48**:3 (2010), 980–1012.

[5] C. Dawson, S. Sun, and M. F. Wheeler, *Compatible algorithms for coupled flow and transport*, Computer Methods in Applied Mechanics and Engineering **193**:23 (2004), 2565–2580.

[6] G. A. Francfort and J.-J. Marigo, *Revisiting brittle fracture as an energy minimization problem*, Journal of the Mechanics and Physics of Solids **46**:8 (1998), 1319–1342.

[7] T. Heister, M. F. Wheeler, and T. Wick, *A primal-dual active set method and predictor-corrector mesh adaptivity for computing fracture propagation using a phase-field approach*, Computer Methods in Applied Mechanics and Engineering **290** (2015), 466–495.

[8] C. MIEHE, F. WELSCHINGER, AND M. HOFACKER, *Thermodynamically consistent phase-field models of fracture: Variational principles and multi-field fe implementations*, International Journal for Numerical Methods in Engineering **83**:10 (2010), 1273–1311.

[9] C. MIEHE, M. HOFACKER, AND F. WELSCHINGER, *A phase field model for rate-independent crack propagation: Robust algorithmic implementation based on operator splits*, Computer Methods in Applied Mechanics and Engineering **199**:45 (2010), 2765–2778.

[10] A. MIKELIĆ, M. F. WHEELER, AND T. WICK, *A quasi-static phase-field approach to pressurized fractures*, Nonlinearity **28**:5 (2015), 1371.

[11] B. RIVIÈRE, *Discontinuous galerkin methods for solving elliptic and parabolic equations: theory and implementation*, SIAM, 2008.

[12] B. RIVIÈRE, M. F. WHEELER, K. BANAŚ, ET AL., *Discontinuous galerkin method applied to a single phase flow in porous media*, Computational Geosciences **4**:4 (2000), 337–349.

[13] S. SUN AND J. LIU, *A locally conservative finite element method based on piecewise constant enrichment of the continuous galerkin method*, SIAM Journal on Scientific Computing **31**:4 (2009), 2528–2548.

[14] M. F. WHEELER, T. WICK, AND W. WOLLNER, *An augmented-lagrangian method for the phase-field approach for pressurized fractures*, Computer Methods in Applied Mechanics and Engineering **271** (2014), 69–85.